Oversampled Receive Array Calibration

Yuri I. Abramovich
WR Systems
Fairfax, VA 22030 USA

Geoffrey San Antonio
US Naval Research Laboratory
Washington, DC 20375 USA

***Abstract*—The problem of receive antenna array calibration in cases where the array is strongly spatially "over-sampled" is addressed in this paper. We suggest a new technique wherein spatially distributed strong clutter returns can be used for calibration with the goal of minimizing the power at the output of a number of antenna finger-beams steered into the invisible domain. The calibration algorithm is analyzed using simulation results and real over-the-horizon radar (OTHR) data to illustrate the effectiveness of the proposed technique.**

I. Introduction

The use of receive antenna arrays in a strong external noise and clutter environment requires very low beampattern sidelobes. In the case of over-the-horizon radar (OTHR) [1], with the typical receive antenna dimensions of 2-3km, the problem of antenna calibration is far from trivial. Normally, complex calibration signal distribution networks are used within the receive array to perform a first order calibration of the individual receivers [3]. These types of calibration techniques do not correct for errors external to the physical receivers. This necessitates the use of external calibration sources with certain requirements.

External calibration sources should be sufficiently far away to operate in the antenna array far-field, but at the same time their signal strength needs to be rather strong and sufficiently clean. Typical ionospheric propagation via a skywave is often corrupted by multimode or phase instabilities, thus causing its wavefront purity/cleanness to be degraded. Moreover, in order to achieve high peak-to-sidelobe ratios, the calibration signal-to-noise ratio should be within the same dynamic range, which means the calibration signal should be exceptionally strong; a source in excess of 40dB SNR would be required to achieve calibrated sidelobes on the order of -40dBc. These quite contradictory requirements make it difficult to obtain a calibration test signal across the entire HF (3-30MHz) band.

At higher frequencies above 20MHz, in [2] a calibration procedure was proposed where full power HF backscatter reflections from large orbiting objects, and in particular the International Space Station (ISS), were used to calibrate an HF OTHR receive array. Such a calibration procedure can only be performed at night well above the maximal usable frequency (MUF), when the impact of the ionosphere can be ignored. Practical experiments have produced quite encouraging results, despite the still observed sphericity of backscattered wavefronts and polarization fading phenomena [2]. Other authors have proposed similar calibration techniques using special purpose space calibration objects [4]. A detailed background on all previous calibration methods applied to OTHR is beyond the scope of this paper. The interested reader is directed to [5], [6] as a starting point.

Obviously, the above mentioned calibration approach using spaced based objects is completely inappropriate for nighttime frequencies where strong ionospheric propagation exists both day and night. It is also impractical to consider the installation of several high power (kW level) dedicated source calibration sources within the radar field of regard. If anything, the quality of antenna calibration at these lower frequencies needs to be better due to the significantly more powerful ambient noise level (lower sidelobe requirement) [7].

In this paper we will introduce an array calibration technique that exploits significant array spatial over-sampling rates (d = [λ/10, λ/5]). The requirements are a) clutter power should be present at almost every visible angle and b) a powerful enough transmit illuminator should be available to produce strong CNR (clutter-to-noise ratio) on a per element basis at the receive array. The application discussed in this paper is with respect to a one-dimensional uniformly sampled receive array, however the same method can be applied to two-dimensional over-sampled arrays. Exact requirements for spatial oversampling rates and required SNR will be explored through simulation examples. Section II presents the over-sampled array calibration technique. Section III presents selected simulated and real data results. Section IV includes concluding remarks.

II. Calibration Methodology for Over-Sampled HF Receive Antenna Arrays

Consider an N-element uniform linear antenna array (ULA) with inter-element spacing d = λ/ℓ, $\ell = 2\rho$ ($\rho \in [3, 5]$, typical oversampling rate for OTHR receive array in the lower HF band). The initial treatment of the problem will assume that none of the array elements are faulty and only unknown amplitude and phase errors exist due to poor antenna calibration. Under these assumptions, the antenna array manifold vector $\mathbf{a}(\theta)$ may be represented as [13]:

$$\mathbf{a}(\theta) = \mathbf{D}_e \mathbf{Z} \mathbf{s}_{id}(\theta), \tag{1}$$

where

$$\mathbf{s}_{id}(\theta) = [1, e^{j2\pi \frac{d}{\lambda} \sin(\theta)}, \ldots, e^{j(N-1)2\pi \frac{d}{\lambda} \sin(\theta)}]^T, \tag{2}$$

$$\mathbf{e}_r = [(1+a_1)e^{j\phi_1}, (1+a_2)e^{j\phi_2}, \ldots, (1+a_N)e^{j\phi_N}]^T, \tag{3}$$

978-0-9928626-3-3/15/$31.00 ©2015 IEEE

and

$$\mathbf{D}_e = diag(\mathbf{e}_r). \tag{4}$$

The notation $diag(\mathbf{e}_r)$ refers to a diagonal matrix built with the vector $\mathbf{e}_r$. Here $\mathbf{Z} \in \mathbb{C}^{N\times N}$ is the mutual coupling matrix that should be always considered for oversampled antenna arrays. In most cases this is a banded matrix due to the physical electromagnetic coupling of a single antenna element with a limited number of surrounding elements. The number of coupled elements does not exceed $\lambda/2d$ (at every side of the ULA element). In this study, similarly to [14], we consider homogeneous mutual coupling as when the matrix $\mathbf{Z}$ is a band Toeplitz matrix, with the width of this band equal to 2k+1≪N. It is straightforward to show that apart from the k edge elements of the oversampled ULA, the following equation is true

$$\mathbf{s}(\theta) = \mathbf{T}\mathbf{s}_{id}(\theta) \overset{k}{=} \mathbf{Z}\mathbf{s}_{id}(\theta) \tag{5}$$

where the introduced symbol $\overset{k}{=}$ means strict equality for all elements of the N-variate vector, excluding the first and last k elements. The matrix $\mathbf{T}$ is a diagonal array spatial taper matrix. A similar matrix is defined later in (14).

For this reason, a number (k) of so-called "dummy" antenna elements are often used to augment operational N-element antenna arrays in order to make this operational N-element array fully homogeneous, with the equation,

$$\mathbf{a}(\theta) = \mathbf{D}_e\mathbf{s}_{id}(\theta) \tag{6}$$

true for all N elements of this array, irrespective of homogeneous mutual coupling. Another option is to apply a heavy taper that significantly reduces contributions of the edge antenna elements. Both reasons allow us to ignore the homogeneous mutual coupling in our efforts to calibrate out the amplitude and phase errors (a_i,ϕ_i) that occur in the antenna multichannel feeder, LNA, and receiver systems. For non-homogeneous mutual coupling described by a non-Toeplitz mutual coupling matrix, the calibration problem is more complex and will be addressed separately. For the model given in (6), we will use $\mathbf{s}(\theta)$ instead of $\mathbf{s}_{id}(\theta)$ and note that (6) may be equivalently introduced as

$$\mathbf{a}(\theta) = diag(\mathbf{s}(\theta))\mathbf{e}_r, \tag{7}$$

and we will use this equivalent representation in derivation that follows.

Consider the spatial frequency

$$\mu = 2\pi\frac{d}{\lambda}\sin(\theta) = \frac{\pi}{\rho}\sin(\theta). \tag{8}$$

The area of "visible" angles $-90^o \leq \theta \leq 90^o$, calculated from the boresight direction, corresponds to $|\mu| \leq \frac{\pi}{\rho}$, while spatial frequencies within the range $\frac{\pi}{\rho} \leq |\mu| \leq \pi$ correspond to "invisible" angles. Let us assume that the arc of visible angles

$$-\frac{\Omega_0}{2} \leq \mu \leq \frac{\Omega_0}{2}, \Omega_0 = \frac{2\pi}{\rho} \tag{9}$$

is uniformly occupied by strong clutter with power σ_c^2. To be clear, the term "invisible" angles corresponds to that part of the unambiguous spatial frequency spectrum that does not correspond to any possible real-world spatial source location [8]. Let each receive element have internal white noise power σ_n^2 which is uncorrelated between receivers. Even though the sources of internal noise are independent, due to mutual coupling the actual noise at the output of the multichannel receiver is correlated with a hermitian covariance matrix $\sigma_n^2\mathbf{R}_n$ [13]. Similarly, each receiver is corrupted by spatially homogeneous external white noise with power σ_{ext}^2. This term can be subsumed into the clutter power component as they both are spatially homogeneous and emanate only from the visible region. This is in contrast to internal noise which appears to emanate from both the visible and invisible regions.

Then the covariance matrix of the internal noise and clutter at the output of the actual antenna array may be presented as

$$\mathbf{R}_{cr}(\Omega_0) = \mathbf{D}_e(\sigma_c^2\mathbf{C}_c(\Omega_0) + \sigma_n^2\mathbf{R}_n)\mathbf{D}_e^H, \tag{10}$$

where the NxN matrix of the clutter covariance is defined as

$$\mathbf{C}_c(\Omega_0)_{j,k} = 2\int_0^{\Omega_0/2}\cos(\mu(j-k))d\mu \qquad j,k = \{0,1,\ldots,N-1\}. \tag{11}$$

This form for the clutter covariance follows directly from the receive array manifold model (1) and the above mentioned assumption that clutter power impinges on the array from all directions with uniform power. More formally, the clutter plus noise covariance could defined in terms of the expected value operator. Therefore the components of the clutter covariance can be expressed as

$$\begin{aligned}\mathbf{C}_c(\Omega_0)_{j,k} &= \Omega_0\frac{\sin(\Omega_0/2(j-k))}{\Omega_0/2(j-k)} \\ &= \frac{\Omega_0}{\pi}sinc\left(\frac{\Omega_0}{2\pi}(j-k)\right) \\ &\quad j,k = \{0,1,\ldots,N-1\}\end{aligned} \tag{12}$$

which is the well-known Slepian kernel and $sinc(x) = \sin(x\pi)/x\pi$ [9], [11]. The noise covariance matrix $\mathbf{R}_n$ has been included as a general covariance term because in theory this noise component should exhibit some degree correlation due to coupled internal noise. Further discussion can be found in [10]. Simulated results in this paper utilize an internal noise model dominated by uncorrelated white noise.

It was previously mentioned in the introduction that other calibration techniques which employ line-of-sight objects require compensation for spherical wavefront curvature. This is due to their inherent proximity to the receive array for which far-field signal model assumptions no longer apply. In this paper we assume that all sources of clutter to be used for calibration arrive from sufficiently far ranges so that our far-field model applies. In the skywave OTHR case, this is not too onerous an assumption because typical backscatter clutter is more than 500km in slant range and in addition, proper range gating can be applied to limit the contamination of

possible near-field sources. If however near-field sources were to contaminate the clutter covariance matrix, their effect would be negligible unless their azimuthal location was close to the visible/invisible space boundary. Typical near-field/far-field mismatches cause broadened mainlobes responses not sidelobe distortion. Thus a near-field source located near the visible space boundary could leak excess energy into the invisible region via an overly broadened mainlobe response. Practically, such an event would be very unlikely to occur since real arrays have greatly diminished responses in the endfire direction.

The nominal (for an ideal antenna array with no error) beamsteering vector for the beamsteer direction μ_0 can be written as

$$\mathbf{w}_i(\mu_0) = \mathbf{T}\mathbf{s}(\mu_0), \tag{13}$$

where μ_0 is the beemsteer direction, $-\pi \leq \mu_0 \leq \pi$ and

$$\mathbf{T} = diag([t_1, t_2, \ldots, t_N]) \tag{14}$$

is the "taper" designed to achieve the required (low) sidelobe level in the properly calibrated ULA. Let

$$\mathbf{W}_i(\mu_0) = diag(\mathbf{w}_i(\mu_0)) \tag{15}$$

be the diagonal matrix formed by this ideal beamfomer.

Let a correction $\mathbf{v}_n$ be introduced that can be applied to the ideal beamsteer vector to correct for phase and amplitude errors. The beamsteer vector can then be written as

$$\mathbf{w}(\mu_0) = diag(\mathbf{v}_n)\mathbf{T}\mathbf{s}(\mu_0), \tag{16}$$

or equivalently,

$$\mathbf{w}(\mu_0) = diag(\mathbf{s}(\mu_0))\mathbf{T}\mathbf{v}_n. \tag{17}$$

If we introduce the notation

$$\mathbf{S}(\mu_0) = diag(\mathbf{s}(\mu_0)), \tag{18}$$

then the output power for the beamformer in (17) is equal to

$$\begin{aligned} p(\mu_0) &= \mathbf{w}^H(\mu_0)\mathbf{R}_{cr}(\Omega_0)\mathbf{w}(\mu_0) \\ &= \mathbf{v}_n^H\mathbf{T}^H\mathbf{S}^H(\mu_0)\mathbf{D}_e(\sigma_c^2\mathbf{C}_c(\Omega_0) + \sigma_n^2\mathbf{R}_n)\mathbf{D}_e^H\mathbf{S}(\mu_0)\mathbf{T}\mathbf{v}_n. \end{aligned} \tag{19}$$

Since $\mathbf{T}$, $\mathbf{S}(\mu_0)$, and $\mathbf{D}_e$ are all diagonal matrices and therefore commuting matrices, (19) could be written as

$$\begin{aligned} p(\mu_0) &= \mathbf{w}^H(\mu_0)\mathbf{R}_{cr}(\Omega_0)\mathbf{w}(\mu_0) \\ &= \mathbf{v}_n^H\mathbf{D}_e\mathbf{T}^H\mathbf{S}^H(\mu_0)(\sigma_c^2\mathbf{C}_c(\Omega_0) + \sigma_n^2\mathbf{R}_n)\mathbf{S}(\mu_0)\mathbf{T}\mathbf{D}_e^H\mathbf{v}_n. \end{aligned} \tag{20}$$

Now let

$$\mu_j \in [-\pi, -\frac{\pi}{\rho}] \cup [\frac{\pi}{\rho}, \pi], j = 1, \ldots, J \tag{21}$$

correspond to a dense sampling of steer directions that populate the entire invisible region. Then the total power due to the output of all these beams will be

$$\begin{aligned} P_{inv} &= \frac{1}{J}\sum_{j=1}^{J}\mathbf{w}^H(\mu_j)\mathbf{R}_{cr}(\Omega_0)\mathbf{w}(\mu_j) \\ &= \mathbf{v}_n^H\mathbf{D}_e\mathbf{T}^H(\sigma_c^2\mathbf{C} + \sigma_n^2\mathbf{R}_n^{inv})\mathbf{T}\mathbf{D}_e^H\mathbf{v}_n. \end{aligned} \tag{22}$$

where

$$\mathbf{C} = \frac{1}{J}\sum_{j=1}^{J}\mathbf{S}^H(\mu_j)\mathbf{C}_c(\Omega_0)\mathbf{S}(\mu_j) \tag{23}$$

$$\mathbf{R}_n^{inv} = \frac{1}{J}\sum_{j=1}^{J}\mathbf{S}^H(\mu_j)\mathbf{R}_n(\Omega_0)\mathbf{S}(\mu_j). \tag{24}$$

Note, it is important to correctly normalize (23) so that correct absolute thresholds can be applied at later processing steps. In the limit as all invisible space points are sampled (23) can be expressed as

$$\begin{aligned} \mathbf{C}_{j,k} &= \mathbf{C}_c(\Omega_0)_{j,k} \cdot \frac{1}{\pi - \frac{\pi}{\rho}}\int_{\pi/\rho}^{\pi}\cos(\mu(k-j))d\mu \\ j,k &= \{0, 1, \ldots, N-1\}. \end{aligned} \tag{25}$$

The covariance can be further simplified to

$$\begin{aligned} \mathbf{C}_{j,k} &= \mathbf{C}_c(\Omega_0)_{j,k}\frac{\rho}{\rho - 1}\left(1_{j-k} - \frac{1}{\rho}sinc\left(\frac{1}{\rho}(j-k)\right)\right) \\ &= \frac{\Omega_0\rho}{\pi(\rho-1)}\left(1_l - \frac{1}{\rho}sinc\left(\frac{l}{\rho}\right)\right)sinc\left(\frac{\Omega_0}{2\rho}l\right) \end{aligned} \tag{26}$$

$$\begin{aligned} l &= j - k, \\ 1_{j-k} &= \delta(j-k). \end{aligned} \tag{27}$$

The above expression for the kernel (23) and (26) is only exact if the clutter distribution is perfectly uniform. It has been included for completeness as it is used in some of the simulation results that will follow. In practice, this kernel is estimated from training data. From (23) and (26) it follows that by collecting the total power within the invisible area, we are in fact collecting power of all the beampattern sidelobes, except for the invisible region arc,

$$\frac{\Omega_0}{2} \leq \mid \mu \mid \leq \frac{\pi}{\rho}. \tag{28}$$

Therefore, if strong clutter (and/or other interferers) occupy the entire visual arc ($\Omega_0/2 = \pi/\rho$), then all the visual arc sidelobes are represented in (23) and (26). Otherwise, sidelobes from the arc (28) are not represented by the kernel (23) and (26). The calibration vector $\mathbf{v}_n$ that minimizes the expression (22) is simply the minimum eigenvector of the kernel expressed in (23) and (26).

Let us now consider the power output of (20) due to the receiver noise component. Consider an uncalibrated beam steered into the invisible region in the absence of clutter power. In this case the calibration vector $\mathbf{v}_n$ is set to $\mathbf{e}_n = [1, 1, \ldots, 1]^T$, the all ones vector. The resulting noise power is

$$\sigma_{int}^2 = \mathbf{e}_n^H\mathbf{D}_e\mathbf{T}^H\mathbf{R}_n^{inv}\mathbf{T}\mathbf{D}_e^H\mathbf{e}_n\sigma_n^2. \tag{29}$$

Estimation of this noise power can be accomplished by collecting data during a "quiet" dwell, with the transmitter switched off. This estimate of (29) will perform reasonably well as long as the external-to-internal noise ratio $\sigma_{ext}^2/\sigma_n^2$ does not exceed the peak-to-sidelobe ratio of the original uncalibrated antenna array. Otherwise an estimate σ_{tr}^2 of the

invisible space power level should be used which can be derived from the data containing clutter returns.

$$\sigma_{tr}^2 = \alpha \mathbf{e}_n^T \left(\frac{1}{J} \sum_{j=1}^{J} \mathbf{W}^H(\mu_j) \mathbf{R}_{cr}(\Omega_0) \mathbf{W}(\mu_j) \right) \mathbf{e}_n \quad (30)$$

where α is the designed level of beampattern sidelobes.

Now let $\mathbf{U}_K = [\mathbf{u}_1, \mathbf{u}_2, \ldots, \mathbf{u}_K] \in \mathcal{C}^{NxK}$ be the matrix of K smallest eigenvectors of the kernel matrix in (22), where K is selected according to the condition

$$\sum_{j=1}^{K} \lambda_j \mathbf{e}_n^T \mathbf{u}_j \mathbf{u}_j^H \mathbf{e}_n \approx \begin{cases} \sigma_{int}^2, \text{ if available} \\ \sigma_{tr}^2, \text{ otherwise} \end{cases} \quad (31)$$

and $\{\lambda_1, \ldots, \lambda_K\}$ corresponds to the K smallest eigenvalues of the aforementioned kernel arranged in ascending order. This condition means that with the correction vector $\mathbf{v}_{opt}(K)$ defined as

$$\mathbf{v}_{opt}(K) = \mathbf{U}_K \mathbf{U}_K^H \mathbf{e}_n \quad (32)$$

we obtain the total power collected by the beams steered into the invisible domain equal to the power expected for the properly calibrated antenna. Concurrently the vector (32) is the one with the minimal total mean square error deviation from the vector $\mathbf{e}_n$, since

$$\min_{\mathbf{b}_K} \|\mathbf{U}_K \mathbf{b}_K - \mathbf{e}_n\|_2^2, \mathbf{b}_K \in \mathcal{C}^{Kx1} \quad (33)$$

is minimized with $\mathbf{b}_K = \mathbf{U}_K^H \mathbf{e}_n$ and therefore (32) holds.

The following list outlines the steps required to implement the calibration algorithm in practice.

Calibration Algorithm Steps

1) Collect L array spatial snapshots $\mathbf{X} = [\mathbf{x}_1, \ldots, \mathbf{x}_L]$ containing strong clutter power from all azimuths.
2) Form array spatial covariance estimate $\hat{\mathbf{R}} = \frac{1}{L} \mathbf{X}\mathbf{X}^H$.
3) Compute the kernel $\mathbf{C}$ defined in (23) with the estimated array spatial covariance substituted for the assumed model.
4) Apply the desired array taper to the computed kernel $\mathbf{C}_T = \mathbf{T}^H \mathbf{C} \mathbf{T}$ then find the eigenvectors $\mathbf{U}$ and eigenvalues $\mathbf{\Lambda}$ of this matrix.
5) Finally compute the correction according to (32) utilizing the known or estimated internal noise level to find K according to (31).

III. Results

In this section we will examine the performance of the proposed array calibration method through simulation and real data results. The following areas have been explored, but not all are discussed due to space limitations: Subspace dimension approximation, element CNR, frequency dependence, visible region illumination coverage, and number of array snapshots. In the simulations, the clutter has been generated by using a simple far-field free space propagation model. No attempt has been made to include ionospheric propagation effects. This simple analysis method appears justifiable because no strange ionospheric effects will adversely impact the algorithm performance. Results using real data are further evidence of this statement.

It is expected that there should be a strong dependence of the accuracy of the calibration solution on the element level CNR. Intuitively, one would expect the calibration accuracy to suffer as the CNR level is decreased. Figure 1 shows the result for CNR=50dB. At CNR=50dB we are close to achieving near perfect calibration. The calibration results for CNR=30dB (not shown) are decreased, but still very respectable. The basic requirement is that enough CNR is required so that the beampattern sidelobes are sufficiently visible in invisible space above the internal noise floor. As mentioned in the theoretical development, it is important to collect clutter power from nearly all visible azimuth angles. One solution to acheive uniform transmit illumination would be to use a single broad coverage low power transmit antenna for calibration purposes. However, an alternative could be to utilize a sequence of stepped scanned narrow beam transmit beampatterns. Such a method is applicable to high-power OTHR transmit phased arrays. To illustrate the concept a simulation was run in which a broad illumination pattern has been synthesized using 10 narrow beam transmit patterns stepped 10 degrees in azimuth from $\pm 45^o$. The result is shown in Fig. 2. Notice that the broadened illumination pattern has restored a large amount of the visible region sidelobe levels. We conclude by showing the performance of the calibration algorithm on a real HF receive array. The data was collected using a N=100 element system without any bad elements. The collection was performed using a high-power far field illumination source to act as a surrogate plane wave emitter. The receive array has the same spacing as used in the simulations in the previous section and data was collected at 7.93MHz. Training data was collected by sequentially illuminating 10 dwell regions spaced 10 degrees in azimuth. A total of 5 multi-dwell sets were used. The result of the calibration solution is shown in Fig. 3. First note that the illumination source propagated over a multi-mode path and as such there is not a single clean plane wave impinging on the receive array. In this example normal system calibration has been applied prior to the application of the improved calibration solution. The uncalibrated solution is shown with the circle trace. The average sidelobe level is well above -40dB for all angles. Some regions of the invisible space contain sidelobes as high as -30dB. Once the calibration solution is applied, the sidelobes are reduced about 15dB in both the visible and invisible regions. The designed ideal taper has its first sidelobes 60dB down. The calibration solution provides a great improvement, however there may still be further improvements that can be made if more advanced calibration methods are employed.

IV. Conclusion

This paper has presented a new receive array calibration technique for spatially oversampled arrays. HF OTHR has been the primary motivation for this work, however there is no reason why the same algorithm can not be applied to more general array applications. The operation of the algorithm has

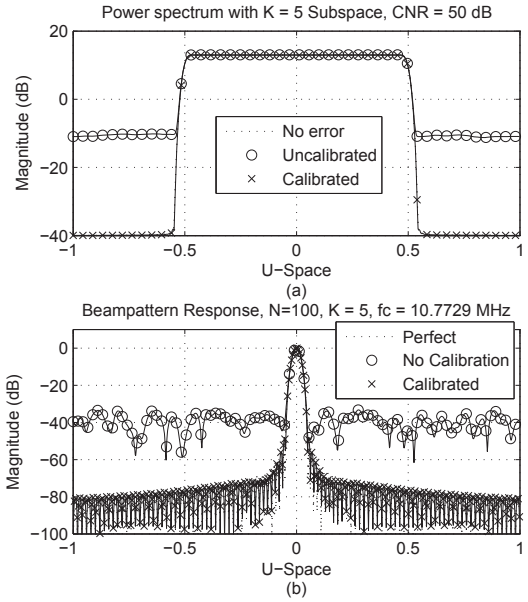

Fig. 1. Calibration solution using CNR=50dB. (a) Beamformer output power as a function of all u-space angles. (b) Beampattern response for no errors, no calibration, and estimated calibration. Note, invisible space region begins at |u|=0.5.

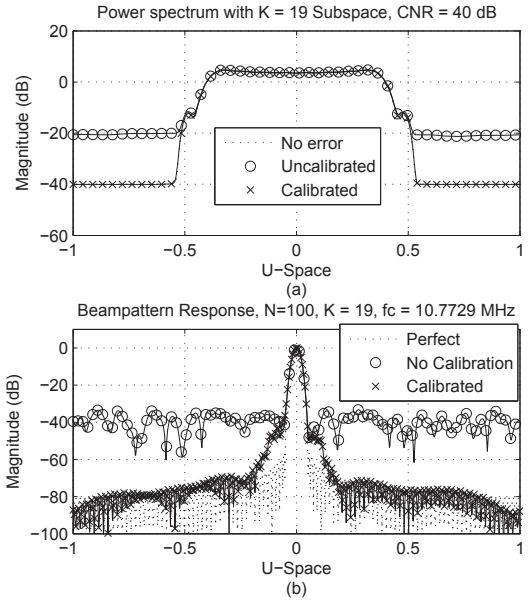

Fig. 2. Calibration solution using 10 narrow transmit beams spaced 10 degrees in azimuth. Beampattern response for no errors, no calibration, and estimated calibration. Note, invisible space region begins at |u|=0.5.

been verified using both simulated and real HF OTHR data. A key feature of the proposed calibration algorithm is that it does not require the presence of a cooperative far-field source. Rather, normal backscatter clutter data can be used for calibration which can significantly reduce the scheduling burden imposed by normal array calibration.

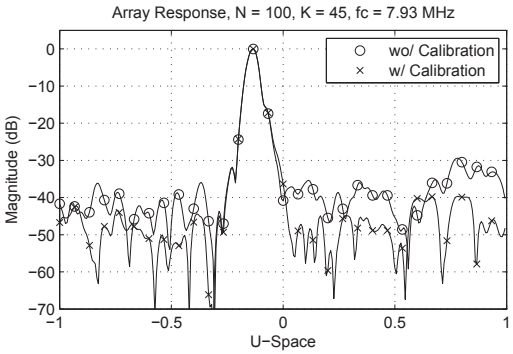

Fig. 3. Real data calibration solution. Far-field illumination source has been used to generate a plane wave source to examine array sidelobes. The no calibration solution does include normal system calibration. Note, invisible space region begins at |u|=0.36.

ACKNOWLEDGMENT

This work was sponsored by the Office of Naval Research under an NRL 6.1 Base Program. The authors would like to thank Dan Sullivan of the Raytheon Corperation for assisting with the data collection.

REFERENCES

[1] J. M. Headrick and S. J. Anderson, "HF Over-the-Horizon Radar," in *Radar Handbook*, 3rd ed., M. Skolnik, Ed. New York: McGraw-Hill, 2008, ch. 20.

[2] S. G. McMillan, "OTH Radar Array Calibration Using LOS Active Returns (ORACULAR)," M.S. thesis, Dept. Elec. Eng., Univ. Adelaide, Adelaide, Aus., 2011.

[3] T. H. Pearce, "Calibration of a Large Receiving Array for HF Radar," HF Radio Systems and Techniques, Nottingham, UK, 7-10 July 1997, pp. 260-264.

[4] P. A. Bernhardt and C. L. Siefring and J. F. Thomason and S. P. Rodriquez and A. C. Nicholas and S. M. Koss and M. Nurnberger and C. Hoberman and M. Davis and D. L. Hysell and M. C. Kelley, "The Design and Applications of a Versatile HF Radar Calibration Target in Low Earth Orbit," *Radio Science*, vol. 43, RS1010, doi:10.1029/2007RS003692, 2008.

[5] I. S. D. Solomon, "Over-the-Horizon Radar Array Calibration," Ph.D. dissertation, Dept. Elec. Eng., Univ. Adelaide, Adelaide, Aus., 1998.

[6] I. S. D. Solomon and D. A. Gray and Y. I. Abramovich and S. J. Anderson, "Receiver Array Calibration Using Disparate Sources," *IEEE Trans. Ant. and Prop.*, vol. 47, No. 3, pp. 496-505, 1999.

[7] International Radio Consultive Committee (CCIR) Report 322-3, "Characteristics and Applications of Atmospheric Radio Noise Data," Documents of the XVth Plenary Assembly, Geneva, 1983.

[8] W. L. Stutzman and G. A. Thiele, *Antenna Theory and Design*, New York, John Wiley, 1981.

[9] D. Slepian, "Prolate Spheroidal Wave Functions, Fourier Analysis and Uncertainty - I," *Bell Sys. Tech. Jour.*, vol. 40, pp. 43-63, 1961.

[10] Y. I Abramovich and G. S. San Antonio, "Network Theory-Based Generic Model for Oversampled Receive Antenna Arrays," SAM 2012 Conf., Hoboken, New Jersey, 17-22 June 2012.

[11] H. L. Van Trees, *Optimum Array Processing*, New York: Wiley-Interscience, 2002.

[12] S. Boyd and L. Vandenberghe, *Convex Optimization*, Cambridge, Engalnd: Cambridge University Press, 2004.

[13] K. F. Warnick and M. A. Jensen, "Optimal Noise Matching for Mutually Coupled Arrays," *IEEE Trans. Ant. and Prop.*, vol. 55, No. 6, pp. 1726-1731, 2007.

[14] B. Friedlander and A. J. Weiss, "Direction Finding in the Presence of Mutual Coupling," *IEEE Trans. Ant. and Prop.*, vol. 39, No. 3, pp. 273-284, 1991.